RADIATION RESEARCH **157**, 92–98 (2002)
0033-7587/02 $5.00

Distributions of Specific Energy in Sensitive Layers of the Human Respiratory Tract

D. Nikezic[1] and K. N. Yu[2]

Department of Physics and Materials Science, City University of Hong Kong, Tat Chee Avenue, Kowloon Tong, Kowloon, Hong Kong

Nikezic, D. and Yu, K. N. Distributions of Specific Energy in Sensitive Layers of the Human Respiratory Tract. *Radiat. Res.* 157, 92–98 (2002).

The purpose of the present work was to calculate the specific energy distribution in sensitive cells of the human lung. Specific energy distributions were calculated by applying Monte Carlo methods and the ICRP 66 model of the human respiratory tract. Specific energies were calculated at various depths in the epithelium and combined according to the relative cell abundance. Distributions are given for various combinations of sources, α-particle energies, targets and regions of the lung. The chord length does not follow the triangular distribution when the particle range is comparable to the diameter of the target. The notion of "effective volume" is introduced and defined, which is needed for estimation of hit frequency in some particular targets. It has been shown that basal cells are subjected to a larger proportion of α-particle hits with small energy transfer than secretory cells. Small energy transfer events that lead to minor damage of the DNA are more efficient in cancer induction than are hits with large energy deposition that lead to cell killing.

INTRODUCTION

The absorbed doses in secretory and basal cells of the human tracheo-bronchial tree have been determined by many authors in the past (*1–5*). These target cells are those from which radiation-induced lung cancers are thought to arise (*2*). A comprehensive report issued by the International Commission on Radiological Protection (ICRP) (*6*) recommends a general approach to calculating the absorbed dose that consists of several steps: (a) determination of the number N_α of α particles emitted from the radon progeny ^{218}Po and ^{214}Bi/^{214}Po in the inner surfaces of the airway tubes for defined exposure conditions and time; (b) multiplication of $N_\alpha E_\alpha$ by the absorbed fractions, AF, of α particles in target tissues (E_α is the α-particle energy); and (c) weighting the doses. In such an approach, the doses are calculated in the layers where the sensitive cells exist; the calculations assume that the doses in the sensitive cells are the same as those in the layers. Two types of cells, secretory and basal cells, are considered to be sensitive to α-particle radiation (*6*, *7*). Therefore, the doses are usually calculated for both types of cells, which are then averaged for all the 16 generations (8 in bronchial region + 8 in bronchiolar region) of the tracheo-bronchial tree.

Another possible approach is the microdosimetric method. Some authors have applied microdosimetry to calculate distributions of microdosimetric quantities in the human lung (*8–12*). The main quantity in microdosimetry is the specific energy, *z*, which is defined as the ratio of energy ε imparted by radiation to a small target site to the mass of that site (*13*). Specific energy is stochastic and is a highly variable quantity. The unit of specific energy is J/kg = Gy.

In the present work, we consider the irradiation of basal and secretory cell nuclei in the wall of an airway tube in the tracheo-bronchial tree by α particles emitted from short-lived radon progeny and calculate the specific energy distributions. All calculations are performed using the morphometric model of the human lung and the airway wall model proposed by ICRP (*6*).

METHODOLOGY

Effective Volume

The Monte Carlo method has been used widely to study radiation transport in different media and geometries, and to investigate a variety of problems where randomness is involved. The present description will focus particularly on the concept of the effective volume, which will be employed in the present work but has not been explored by other investigators.

The first step is the determination of an effective volume in a medium (which is tissue in the present work). Alpha particles emitted from this effective volume have non-zero probabilities of hitting the target (a sphere or some regions) of interest. In contrast, α particles emitted from outside the effective volume have zero probability of hitting the target of interest. In the course of Monte Carlo simulations, the α-particle starting points are sampled *only* in the effective volume. The effective volume is needed to determine the number of hits N_{hit} of the target for a volumetric activity A_v and a time t of irradiation through the following:

$$N_{\text{hit}} = (\varepsilon_{\text{far}} V_{\text{far}} + \varepsilon_{\text{near}} V_{\text{near}}) t A_v, \quad (1)$$

[1] On leave from University of Kragujevac, Faculty of Science, 34000 Kragujevac, Yugoslavia.

[2] Author to whom correspondence should be addressed at Department of Physics and Materials Science, City University of Hong Kong, Tat Chee Avenue, Kowloon Tong, Kowloon, Hong Kong; e-mail: peter.yu@cityu.edu.hk.

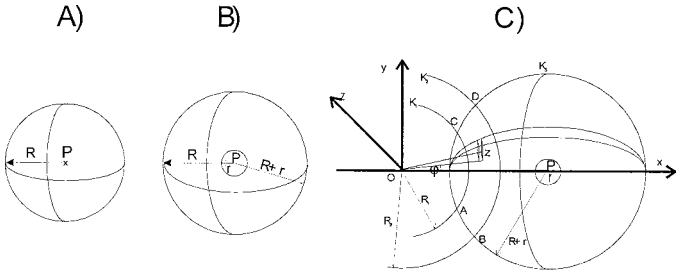

FIG. 1. Effective volume. (A) The effective volume for point P in a homogeneous medium is a sphere centered at point P in which the dose is calculated. The radius R of the sphere is equal to the particle range in the medium. (B) The dose is calculated in a small sphere with radius r and centered at point P. The effective volume is the sphere with radius $r + R$ and centered at P. (C) Effective volume for ''near-wall'' cases. The α-particle source is distributed between cylinders, which are represented in the plane $x = 0$, $y = 0$ by circles K_1 and K_2 with radii R_1 and R_2. The dose is calculated in a cell nucleus represented by a small sphere with radius r and centered at P with coordinates (x_0, 0, 0). The circle K_3 represents the sphere with radius $R + r$ and centered at P. Points A, B, C and D are intersections of circles K_1 and K_2 with the circle K_3. The effective volume is the volume between the surface ABCD and the sphere with radius $R + r$ and centered at P. The same effective volume exists for negative values of z.

where ε_{far} and ε_{near} are efficiencies to hit the target from the far wall and the near wall, and V_{far} and V_{near} are the effective volumes in the far and near walls, respectively. Far-wall cases are those in which α particles cross the air cavity in the tube. If $A_v = 1$ Bq μm^{-3}, and the irradiation time $t = 1$ s, the hit frequency in the unit number of hits per second per Bq μm^{-3} is obtained. The efficiencies ε_i are calculated by Monte Carlo methods. If A_v is known from the modeling of the lung dosimetry, the number of hits in a defined target can be calculated from Eq. (1). The latter quantity will be used for calculations of the specific-energy distribution for a defined exposure condition, e.g. 1 WLM.

In a homogeneous and continuous medium, the effective volume can be defined easily in the following way. If the α-particle dose is calculated at a point P, the effective volume is a sphere with the center at that point and with a radius R equal to the α-particle range in that medium (e.g. tissue); this is illustrated in Fig. 1A. If the dose is calculated in a test sphere with radius r (e.g. a spherical cell nucleus) around a particular point, the effective volume is again the sphere with the center at that point but with the radius $r + R$ (Fig. 1B). When calculations are performed for the airway tube wall, the medium is not homogeneous and continuous. The α-particle source is distributed between two cylinders (e.g., in slow- or fast-moving mucus). The effective volume in this case is obtained as the intersection between the sphere with a diameter $r + R$ and the airway cylinders as shown in Fig. 1C. Determination of the effective volume V_{near} (in μm^3) requires integration of a triple integral as follows:

$$V_{near} = 2 \int\int_{ABCD} \rho \, d\rho \, d\varphi \int_0^{\sqrt{(R+r)^2-\rho^2-x_0^2+2x_0\rho\cos\varphi}} dz, \qquad (2)$$

where x_0 is the x coordinate of the point P, points $ABCD$ are the intersections of the circle K_3 and circles K_1 and K_2 in the plane $x = 0$, $y = 0$ (see Fig. 1C), and ρ and φ are the polar coordinates of the infinitesimal volume element. The origin of the coordinate system is on the axis of the cylinder representing the airway. From Eq. (2), it is seen that the effective volume can be calculated for each depth and particle range. The integral in Eq. (2) is solved numerically by summing the volumes of small elements below the sphere; details of an integration are shown in Fig. 1C. Unexpected numerical problems arise here because of the large difference between the radii of the cylinders (R_1 and R_2) which is of the order of 1000 μm or 5000 μm, the depth of point P in tissue (up to 70 μm), and the small test volume (4–5-μm radius). The details of the numerical calculations performed will not be described in the present paper.

The determination of the effective volume as described above is possible for near-wall cases. For far-wall cases, this is even more complicated, because the medium becomes more inhomogeneous. Part of the α-particle trajectory is in the air, and a tissue-equivalent range has to be used to determine the effective volume for these cases.

Simulation of the Alpha-Particle Transport

The steps for the simulation of α-particle propagation in the airway tube are described briefly here:

(a) The initial directions of the α particles and their starting points in the effective volume are sampled.
(b) If an α particle is not emitted toward the target (point P in Fig. 1), step (a) above is repeated.
(c) The tissue-equivalent distance between the initial point and the entrance point into the target is determined. If the distance is larger than the particle range in tissue, steps (a) and (b) are repeated.
(d) The selected α particle now enters the target. The following sections will describe the determination of microdosimetric and other relevant quantities.
(e) All the above procedures will be repeated until a predetermined number of hits are achieved.

The continuous slowing-down approximation (CSDA) of α particles is used in the calculations. The stopping powers of α particles in striated tissue and air are taken from ref. (*14*).

A computer program based on the above procedures has been developed that calculates the distributions of specific and lineal energy in the target, the distribution of the trajectory length throughout the target, the LET spectra, the fluence and the hit frequencies. Calculations of the quality factor are also possible. A detailed description of the program used in the calculation is beyond the scope of the present paper.

Average Specific Energy, z_{av}, and the Maximum Specific Energy, z_{max}, in the Cell Nucleus per Alpha-Particle Passage

Based on some simplified assumptions, it is possible to estimate the average specific energy, z_{av}, and the maximum specific energy, z_{max}, in a sensitive cell nucleus (for a single hit). If the diameter of the nucleus is 9 μm (*15*), the volume V and the mass m of the nucleus are $V = 4/3\ \pi r^3 = 381$ μm^3, or 381×10^{-12} cm^3, and $m_N = 1.045$ g/cm$^3 \times 381 \times 10^{-12}$ cm^3 $= 398.88 \times 10^{-12}$ g, or 3.9888×10^{-13} kg, where $\rho = 1.045$ g/cm^3 is the tissue density.

The α particles emitted by ^{214}Po have an energy of 7.69 MeV, and their range is approximately 71 μm in tissue. This means that the average stopping power is roughly 0.1 MeV/μm (although the energy deposition is not exactly a linear function of the residual range). Alpha particles which cross the center of the nucleus have a pathlength of 9 μm, and the energy imparted to the nucleus is about 1 MeV. Therefore, the specific energy corresponding to this α-particle passage is $z_{av} = 1$ MeV/$m_N = 0.4$ Gy.

Since the α particles do not generally cross the center, the average specific energy should be smaller than 0.4 Gy. According to ref. (*14*), the maximum stopping power of α particles in tissue is 2400 MeV/cm, or 0.24 MeV/μm. Therefore, the maximum energy of an α particle imparted to the cell nucleus cannot be larger than $9 \times 0.24 = 2.16$ MeV, and the maximum specific energy ε_{max} is given as $z_{max} = 2.16$ MeV/$m_N = 0.8677$ Gy. Because of this, one should not expect to get a specific energy larger than 0.9 Gy for the passage of a single α particle in the nucleus. Even this maximum value is unlikely to be achieved. Larger specific energies can be found only as a result of multiple hits, which are rather rare. Moreover, even if a site is hit more than once, because of cell turnover, this does not necessarily mean that the same cell nucleus has experienced multiple hits.

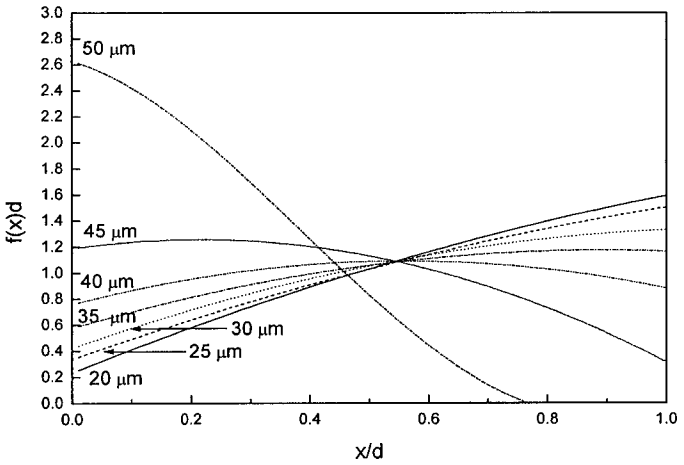

FIG. 2. Distribution of pathlengths in the spherical cell nucleus target with the depth as a parameter. The source of the α particles is in the mucus layer and the initial energy of the α particles is 6 MeV.

Chord Length Distribution

The large variability in the energy imparted to the cell nucleus is attributed to the different lengths of the α-particle paths through the nucleus. It has been shown that the chord lengths of random trajectories through the spherical volume are distributed according to the triangular distribution (*16*):

$$f(x) = \frac{2x}{d^2}, \tag{3}$$

where d is the diameter of the sphere, and $f(x)dx$ is the probability that the chord length through the sphere is between x and $x + dx$.

Equation (3) has been derived under the assumption that all particles entering the spherical volume will traverse it and exit on the opposite side of the sphere. However, this assumption is not correct for cell nuclei irradiated with α particles emitted by radon progeny in the human respiratory tract. The diameter of cell nucleus is about 9 μm, which is not negligible when compared to the range of α particles in tissue (≈47 μm for ^{218}Po and ≈71 μm for ^{214}Po). As a result, some α particles will be stopped in the nuclei, which will affect the previous chord length distribution. A modification of the line predicted by Eq. (3) can be expected because of stopped particles in the spherical volume.

Examples of pathlength distributions are given in Fig. 2. Calculations have been performed for the following input parameters/conditions: (1) an α-particle energy of 6 MeV; (2) a diameter of cell nuclei of 9 μm; (3) the α-particle emitters are situated in the mucus layer which is 5 μm thick (BB1 in ICRP 66 nomenclature); (4) depths of cell nuclei below the top of the mucus varied from 20 μm to 50 μm, with steps of 5 μm.

Similar curves have also been constructed for other α particles arising in other locations (cilia, epithelium, etc.) and having other energies (7.69 MeV). These curves have been used in the calculations of the specific energy distribution.

As the depth increases, the pathlength distribution gradually deviates more from the distribution predicted by Eq. (3). The curves can be decreasing in the deepest region close to the end of the particle range, when no particles can traverse the nucleus. These results show that Eq. (3) cannot be used indiscriminately in the present problem; instead, the establishment of the pathlength distribution is needed for particular depths, sources and energies.

Calculation Schemes and Procedures

Microdosimetry distributions were calculated for epithelial tissues in different regions of sensitive cells, with steps of 5 μm in the bronchial region and 2 μm in the bronchiolar region. All the following elements have been considered and integrated in the calculations: (a) two different regions of the tracheo-bronchial tree according to ICRP 66 (*6*) nomenclature, i.e. bronchial and bronchiolar regions; (b) two different α-particle sources (mucus gel and sol+cilia layer) in each region; (c) two α-particle energies (6 MeV and 7.69 MeV); and (d) two different kinds of sensitive cells (basal and secretory cells) in the bronchial region, and one kind of sensitive cell (secretory cell) in the bronchiolar region.

In contrast to other physicists who performed microdosimetry calculations, we made use of the ICRP 66 (*6*) human respiratory tract model. According to ICRP 66 (*6*) and NRC (*7*), the airway walls in the bronchial region consist of the following layers: 5 μm of mucus gel, 6 μm of sol+cilia, 10 μm of tissue without sensitive cells, 30 μm of secretory cells, and 15 μm of basal cells which partially (5 μm) overlaps with the secretory cells. In the bronchiolar region, the layers are as follows: 2 μm of mucus gel, 4 μm of sol+cilia, 4 μm of tissue without sensitive cells, and 8 μm of secretory cells; there are no basal cells. These structures of the airway wall have been adopted in our calculations.

RESULTS

1. Distributions of specific energy for one event, f_1, have been determined for bronchial and bronchiolar regions for the two α-particle sources (fast- and slow-clearance mucus) and for two α-particle energies involved in the ^{222}Rn decay chain, i.e. 6 MeV and 7.69 MeV.

2. Distributions obtained in various depths of the epithelium have been combined according to the relative number of sensitive cells. The relative numbers of secretory cells and basal cells were taken from ref. (*1*).

3. The 12 one-event distributions f_1 were obtained. Calculations were performed for different combinations of input parameters: The α-particle source was in a fast- or slow-clearance mucus in the bronchial region or the bronchiolar region; the initial α-particle energy was 6 MeV or 7.69 MeV; the targets were basal or secretory cells. Originally, the program gives the one-event distribution for a single α-particle passage through the nucleus. By using the quantity N_{hit} as explained above, the distribution is recalculated for a surface activity of 1 Bq cm^{-2} projected onto the mucus surface.

The probability distributions of the specific energy z were calculated with steps of 5 μm in the bronchial region and 2 μm in the bronchiolar region. For purposes of illustration, some results for 6 MeV α particles are given in Fig. 3 for depths of 20, 30, 40 and 50 μm. Significant changes with the depth can be seen in the z distribution. At a depth of 20 μm, the stretched peak is around $z = 0.3$ Gy. With increasing depth, this peak became less and less visible and finally disappeared, but at the same time a new one appeared at very low values of z. This low-energy peak was prominent at a depth of 50 μm. The result showed that the nature of α-particle interaction with the cell nuclei changed with depth; small energy-transfer events were more probable for basal cells, which extend from 46 to 61 μm below the top surface of the mucus layer.

The results for the f_1 distributions (weighted according to the relative number of the cells) are given in Figs. 4–6 (each with four curves). The distributions for secretory cells in the bronchial region are given in the Fig. 4. The shapes

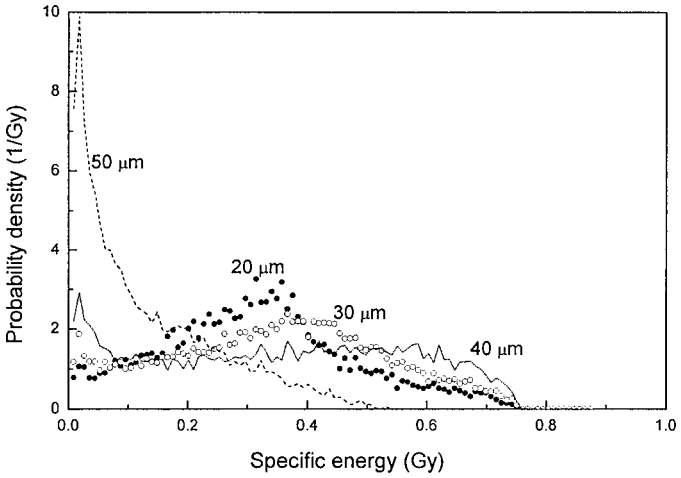

FIG. 3. Monte Carlo results of the probability density distribution f_1 of specific energy in the bronchial region from 6 MeV α particles emitted in the fast-clearance mucus. The depth in the tissue is given as a parameter.

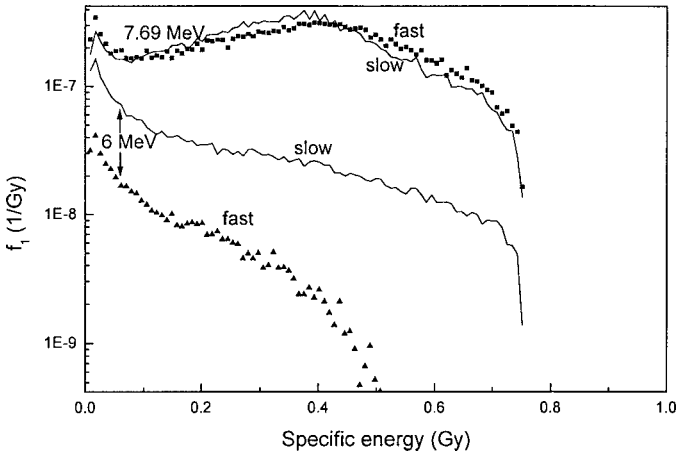

FIG. 5. Monte Carlo results of the one-event distribution of specific energy in basal cells in the bronchial region for an activity of 1 Bq cm^{-2}. The results are given for two initial α-particle energies (6 MeV and 7.69 MeV) and two sources (fast- and slow-clearing mucus). The results are weighted according to the relative number of basal cells given in ref. (*1*).

of the curves are similar to those in Fig. 6 (which gives the results for the bronchiolar region), but the frequencies are smaller than those in Fig. 6 by factors of 3 to 5. The smaller frequencies in the bronchial region are due to the larger distances from the source to the target in the bronchial region, and are also due to the smaller volume abundance of secretory cells in the bronchial region [according to ref. (*1*)].

Figure 5 gives the distribution of specific energy in basal cells in the bronchial region, with a logarithmic scale for the *y* axis. Smaller frequencies were observed than in the previous case. The distributions for the 6 MeV α-particle energy did not show any peaks and decreased monotonically with the specific energy. The distributions for the 7.69 MeV α-particle energy showed a peak at about 0.4 Gy. The significantly smaller frequencies were due to the larger distance from the source to the basal cells than to the secretory cells.

Figure 6 shows the results for secretory cells in the bronchiolar region. Each curve in Fig. 6 shows a peak; the peaks for 7.69 MeV α-particle energy were more prominent and corresponded to smaller *z* values than those for 6 MeV. The curves for the different sources (fast- and slow-clearance mucus) were close to each other, and all the curves merged in the region of large *z* values.

The results in Figs. 4–6 are given for the projected activity of 1 Bq cm^{-2} onto the inner surface of the airway tube. However, the activity for a given exposure was required, so we reported results for the exposure of 1 WLM in additon to the results given in Figs. 4–6. For such calculations, the activity in the mucus gel and sol+cilia layers

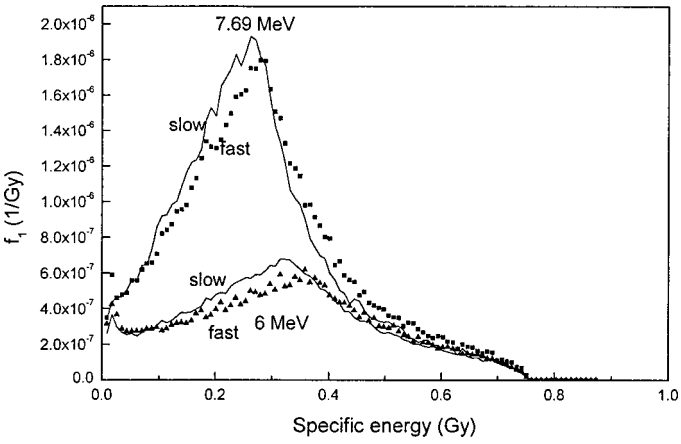

FIG. 4. Monte Carlo results of the one-event distribution of specific energy in secretory cells in the bronchial region for an activity of 1 Bq cm^{-2}. The results are given for two initial α-particle energies (6 MeV and 7.69 MeV) and two sources (fast- and slow-clearing mucus). The scatterplots refer to the fast-clearance mucus, while the solid curves refer to the slow-clearance mucus. The results are weighted according to the relative number of secretory cells given in ref. (*1*).

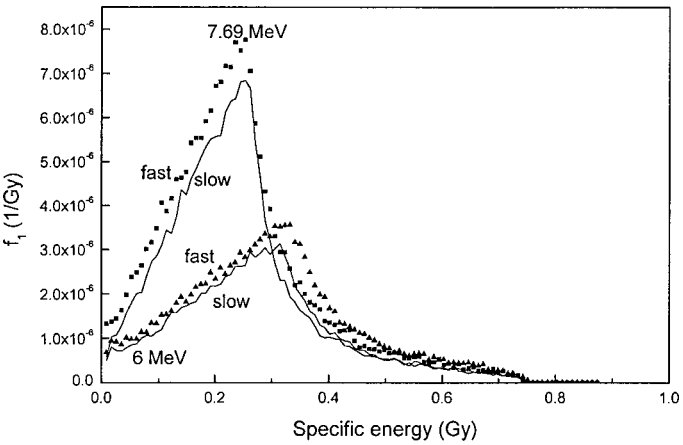

FIG. 6. Monte Carlo results of the one-event distribution of specific energy in the bronchiolar region for an activity of 1 Bq cm^{-2}. Calculations have been made with steps of 5 μm in tissue. The results are weighted according to the relative number of secretory cells given in ref. (*1*).

TABLE 1
Number of α Particles Emitted in Different Regions of the Human Lung (in Disintegrations μm^{-3} per WLM of Exposure)

Alpha-particle source	^{218}Po (6 MeV)	^{214}Po (7.69 MeV)
Bronchi: fast (BB1)	2.352×10^{-5}	7.270×10^{-5}
Bronchi: slow (BB2)	2.022×10^{-5}	6.771×10^{-5}
Bronchioles: fast (bb1)	1.523×10^{-5}	8.845×10^{-5}
Bronchioles: slow (bb2)	0.777×10^{-5}	4.811×10^{-5}

for ''standard'' exposure conditions were needed; these activities were determined by modeling the lung dosimetry

The activities in various sources were calculated using our own computer program called LUNGDOSE. This program is based mainly on ICRP 66 (*6*). We considered the ICRP 66 model the most authoritative one in this field, and our program LUNGDOSE followed it as much as possible. The ICRP 66 model neglected some fine details such as enhanced deposition in the branching regions, abundance and distribution of sensitive cells, etc. Here, one of the fine details, namely the target cell distribution and abundance, given by Mercer *et al.* (*1*) was incorporated into the ICRP 66 model.

The input parameters refer to standard irradiation conditions as follows: breathing rate = 0.78 m^3/h; tidal volume = 0.866 liter/breath; functional residual capacity = 3300 ml; equilibrium factor F = 0.395; unattached fraction of potential α-particle energy concentration f = 8%; density of unattached particles = 1 g/cm^3; density of attached particles = 1.4 g/cm^3; shape factors 1 and 1.1 for unattached and attached particles, respectively; median diameters (with geometrical standard deviations in parentheses) are 0.9 (1.3) nm, 50 (2) nm, 250 (2) nm and 1500 (1.5) nm for unattached particles, nucleation mode, accumulation mode and coarse mode, respectively. This program was used to determine the activities in various compartments of the human lung; the results are given in Table 1. Our program

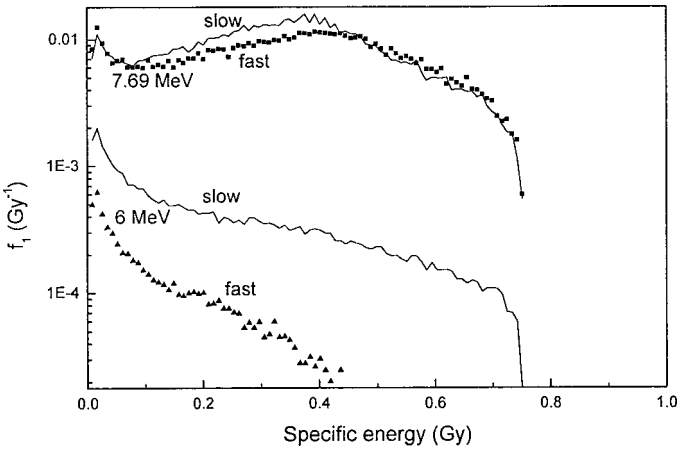

FIG. 8. Monte Carlo results of the one-event distribution of specific energy in basal cells in the bronchial region for an exposure of 1 WLM.

was validated by comparing the values for dose conversion coefficients (effective dose per unit exposure in mSv/WLM) with the values published in ref. (*5*), for which good agreement was obtained (*17*). The success of this program enabled us to make use of intermediate results in the course of calculations of dose conversion coefficients, e.g., the number of α particles emitted in different clearance compartments of the lung.

Figures 7–9 give the specific energy distributions for an exposure of 1 WLM. These results were derived from those of Figs. 4–6 through conversion of the activity of 1 Bq cm^{-2} to the real activity as given in Table 1. Figures 7–9 are similar to Figs. 4–6, but some differences are caused by the different activities of ^{218}Po and ^{214}Po in the sources. These results can be used to calculate the specific energy distributions for other exposure conditions.

DISCUSSION AND CONCLUSIONS

Microdosimetric calculations for radon progeny in the human lung have been performed by Hofmann *et al.* (*12*),

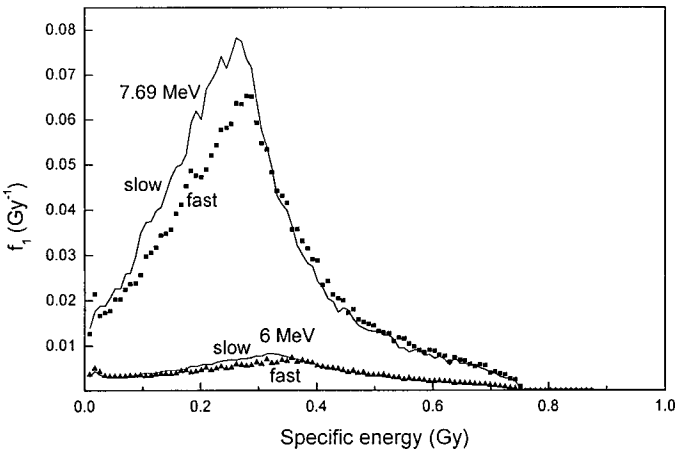

FIG. 7. Monte Carlo results of the one-event distribution of specific energy in secretory cells in the bronchial region for an exposure of 1 WLM.

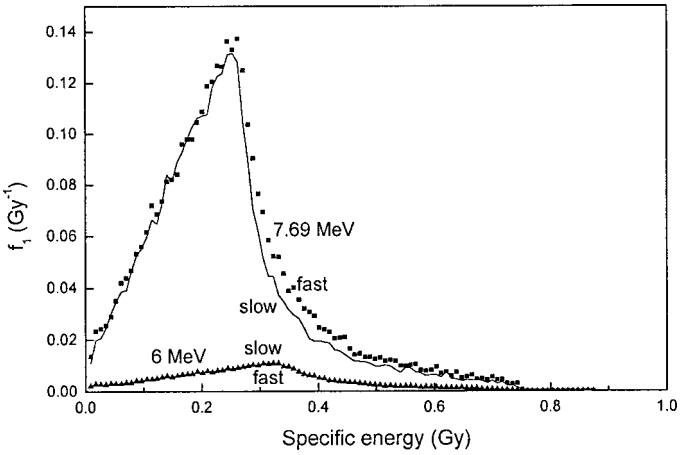

FIG. 9. Monte Carlo results of the one-event distribution of specific energy in secretory cells in the bronchiolar region for an exposure of 1 WLM.

who used the Yeh-Schum morphometry model to calculate the equilibrium activity (in α particles per μm^2) in generations 2, 4, 6 and 10 of the human tracheo-bronchial tree, with a mucus thickness of 15 μm. A similar model was used in another study (*15*). The continuous-slowing-down approximation used to determine the slowing-down spectra of α particles in their work is also adopted in the present work. Here, the microdosimetric distribution of the specific energy was computed, but the equilibrium activity was determined by employing the model of the human respiratory tract in ref. (*6*). We have not considered individual generations of the tracheo-bronchial tree as studied by Hui *et al.* (*8*) and Hofmann *et al.* (*12*). Instead, we follow ICRP 66 (*6*), where the human respiratory tract was divided into five deposition regions.

Distributions of the specific energy have been published (*7*) for two different exposures, 0.023 WLM and 8.45 WLM. Our z distributions are somewhat different; the peaks of our distributions are shifted toward smaller z values between 0.2 and 0.4 Gy, whereas the distributions in ref. (*7*) peaked around 1 Gy. This difference is due to the different applied morphometry and dosimetry models. There are other conceptual differences from ref. (*7*); in that study, the dependence of the basal cell depth x on the airway diameter d was assumed to be $x = 80.8 - 73.8e^{-1.76d}$, while we applied the airway wall model proposed in ref. (*6*). A different cell diameter was also used in the present work. Sedlak (*11*) also made microdosimetric calculations, but used the low-dose data of Hui *et al.* (*8*) to obtain the distribution for the specified dose. Caswell *et al.* (*9*) systematically calculated lineal energy spectra at different depths for various generations, using the continuous slowing-down approximation, the Yeh-Schum morphometry model, and a site diameter of 5 μm. Zaider and Varma (*10*) used the concept of associated surface to calculate the lineal energy distribution, and performed calculations for an airway diameter of 0.3 cm, which corresponded to the Weibel generation 4. The results were given for various ''initial positions'' of α particles in the lung airways and these were not directly comparable with our results.

The results for f_1 distributions for various combinations of source, target, region and energy are given for the hypothetical activity of 1 Bq cm^{-2} on the inner airway surface as well as for the exposure of 1 WLM. The z distributions are different for secretory and basal cells because the latter are situated much deeper in the tissue. The relative number of small energy transfer events is much larger for basal cells than for secretory cells; this is particularly pronounced for 6 MeV α particles. The z distributions for secretory cells (in the bronchial and bronchiolar regions) exhibit very prominent peaks between 0.2 and 0.4 Gy.

The fraction of glancing hits (nonlethal hits with small energy transfers) was larger in basal cells than in secretory cells. A discussion of glancing hits and boundary specific energy (below which a hit is glancing and above which a hit is lethal) can be found in ref. (*11*). Since basal cells are deep in the epithelium, they experience a larger proportion of glancing hits. According to some investigators (*11*), glancing hits can be more efficient in cancer initiation than inactivation (lethal hits). Although the absorbed dose is smaller in basal cells (in the bronchial region) than in secretory cells (in the bronchiolar region), a larger proportion of lung cancers originate in the bronchial region (*6*). A larger proportion of glancing hits to basal cells may explain this.

The characteristics of α-particle interactions are different for basal and secretory cells. This conclusion can be important when the doses in basal cells, $D_{BB,\,basal}$, and those in secretory cells, $D_{BB,\,basal}$, in the bronchial region are weighted to give the total dose in bronchial region, D_{BB}. The weighting scheme $D_{BB} = 0.5D_{BB,\,basal} + 0.5D_{BB,\,basal}$ recommended by ICRP 66 assumes equal importance of doses and thus equal sensitivities for basal and secretory cells (equal weighting factors of 0.5 are used). With the evidence presented here that the α particles interact differently with basal and secretory cells, this weighting scheme might need to be reviewed.

The curves presented here can be useful in the estimation of the cell survival probability T according to (*18*)

$$T = \int e^{z/z_0} f(z)\, dz, \tag{4}$$

where z_0 is the specific energy deposited in the nucleus for which an individual cell has an average survival probability of 1/e.

ACKNOWLEDGMENT

This research was supported by the CERG grant CityU1004/99P from the Research Grant Council of Hong Kong.

Received: January 4, 2001; accepted: August 17, 2001

REFERENCES

1. R. R. Mercer, M. L. Russel and J. D. Crapo, Radon dosimetry based on the depth distribution of nuclei in human and rat lungs. *Health Phys.* **61**, 117–130 (1991).
2. N. H. Harley, Comparing radon daughter dose: Underground vs. environment exposure. *Radiat. Prot. Dosim.* **7**, 371–375 (1984).
3. A. Birchall and A. C. James, Uncertainty analysis of the effective dose per unit exposure from radon progeny and implication for ICRP risk-weighting factors. *Radiat. Prot. Dosim.* **53**, 133–140 (1994).
4. J. Porstendörfer and A. Reineking, Radon: Characteristics in air and dose conversion factors. *Health Phys.* **76**, 300–305 (1999).
5. J. W. Marsh and A. Birchall, Sensitivity analysis of the weighted equivalent lung dose per unit exposure from radon progeny. *Radiat. Prot. Dosim.* **87**, 167–178 (2000).
6. ICRP, *Human Respiratory Tract Model for Radiological Protection.* Report 66, *Annals of the ICRP*, Vol. 24, No. 1–3, Pergamon Press, Oxford, 1994.
7. National Research Council, Panel on Dosimetric Assumptions Affecting the Application of Radon Risk Estimates, *Comparative Dosimetry of Radon in Mines and Homes.* National Academy Press, Washington, DC, 1991.
8. T. E. Hui, J. W. Poston and D. R. Fisher, The microdosimetry of

radon decay products in the respiratory tract. *Radiat. Prot. Dosim.* **31**, 405–411 (1990).

9. R. S. Caswell, L. R. Karam and J. J. Coyne, Systematics of alpha-particle energy spectra and lineal energy (Y) spectra for radon daughters. *Radiat. Prot. Dosim.* **52**, 377–380 (1994).

10. M. Zaider and M. Varma, Carcinogenic risk coefficients at environmental levels of radon exposures: A microdosimetric approach. *Health Phys.* **70**, 837–844 (1996).

11. A. Sedlak, Microdosimetric approach to the problem of lung cancer induced by radon progeny. *Health Phys.* **70**, 680–688 (1996).

12. W. Hofmann, M. Nosterer, M. G. Menache, D. J. Crawford-Brown, R. S. Caswell and J. J. Coyne, Microdosimetry and cellular radiation effects of radon progeny in human bronchial airways. *Radiat. Prot. Dosim.* **52**, 381–385 (1994).

13. A. M. Kellerer, Fundamentals of microdosimetry. In *The Dosimetry of Ionizing Radiation* (K. R. Kase, B. E. Bjorngard and F. H. Attix, Eds.), Vol. 1, pp. 78–162. Academic Press. San Diego, 1985.

14. ICRU, *Stopping Powers and Ranges for Protons and Alpha Particles.* Report 49, International Commission of Radiation Units and Measurements, Bethesda, MD, 1993.

15. W. Hofmann, M. G. Menache, D. J. Crawford-Brown, R. S. Caswell and L. R. Karam, Modeling energy deposition and cellular radiation effects in human bronchial epithelium by radon progeny alpha particles. *Health Phys.* **78**, 377–393 (2000).

16. H. Rossi and M. Zaider, *Microdosimetry and Its Applications.* Springer, Berlin, 1996.

17. D. Nikezic and K. N. Yu, Alpha hit frequency of sensitive cells in T-B tree due to radon progeny. *Int. J. Radiat. Biol.* **77**, 559–565 (2001).

18. T. G. Stinchcomb and J. C. Roeske, Survival of alpha particle irradiated cells as a function of the shape and size of the sensitive volume (nucleus). *Radiat. Prot. Dosim.* **62**, 157–164 (1995).